Multi-scale robust design and optimization considering load uncertainties

Xu Guo[*], Xiaofang Zhao, Weisheng Zhang, Jun Yan, Guomin Sun

Department of Engineering Mechanics, Dalian University of Technology, State Key Laboratory of Structural Analysis for Industrial Equipment, Dalian, 116023, PR China

Abstract

Uncertainty is ubiquitous in practical engineering design applications. Recent years have witnessed a growing research interest in the study of structural topology optimization problems considering uncertainties. Most of these works, however, are focused on the optimization of macro-scale structures. In the present paper, robust concurrent optimization of material and structure under unknown-but-bounded load uncertainties is investigated in a multi-scale framework. Problem formulation that can allow for the effect of worst-case scenario in a confidence way and the corresponding numerical solution procedure are proposed. It is found that when load uncertainties are considered, optimal material distributions in microstructures tend to be isotropic and Kagome structure seems to be superior to other forms of microstructures. The conclusions drawn from the present work are helpful for manufacturing hierarchical structures with Additive Manufacturing technologies.

1. Introduction

Topology optimization, which aims at optimizing available material distribution in a prescribed design, has undergone tremendous development since the pioneering work of Bendsoe and Kikuchi [1]. Nowadays, topology optimization has been used successfully in many industrial fields, such as automotive, aerospace and so on. A state-of-the-art review and some recent developments in this field can be found in the review articles [2–4] and the references therein.

Traditionally, topology optimization has often been applied to design macroscopic structures where a black-and-white material distribution is sought for [4]. Recent years, however, have witnessed an ever increasing research interest in multi-scale material design and optimization, where the material distributions in micro and macro scales are optimized simultaneously. The driving force for the study of multi-scale optimization comes from two sources. The first one is the impetus for designing ultra-light materials with relatively high strength/stiffness–weight ratios. Numerous

---

* Corresponding author. Tel.: +86 411 84707807.
E-mail address: guoxu@dlut.edu.cn (X. Guo).

theoretical and experimental researches [5] reveal that compared with traditional materials (e.g., steel, aluminum and ceramic), ultra-light materials such as truss-like materials, cellular materials or porous foam materials, which have internal microstructures, are superior for multi-functional applications. Therefore if a macroscopic structure is made from cellular materials, it can be expected that if the corresponding microstructure and the macroscopic configuration can be optimized concurrently by taking the interaction between different scales into consideration, then the best overall system performances may be achieved. Another driving force is the rapid development of the modern fabrication techniques which make the manufacturing of ultra-light materials with rather complex microstructures possible. For example, it was reported that with use of self-propagating photopolymer waveguide prototyping approach, ultra-light metallic micro lattice with structural hierarchy at the nanometer, micrometer, and millimeter scales can be fabricated [6]. Although ultra light (density $\rho < 10 \, \mu g/cm^3$), this kind of micro lattice can exhibit complete recovery after compression exceeding 50% strain, and energy absorption similar to elastomers. Furthermore, the emerging Additive Manufacturing technique is also a promising way to fabricate materials with very complex anisotropic microstructures.

Rodrigues et al. first developed a hierarchical numerical scheme for optimizing material distribution as well as the point-wise material microstructures concurrently [7]. In this approach, two inherently coupled problems are solved where the outer problem deals with the spatial distribution of material on macroscopic (global problem) while the inner problem addresses the question of optimal choice of microstructure topology. Liu et al. proposed a so-called PAMP (Porous Anisotropic Material with Penalization) model to optimize the macroscopic and microscopic material distributions simultaneously [8]. In this approach, unlike the treatment in [7], the material microstructure is assumed to be uniform at every macro-scale material point in order to meet manufacturing requirements. Later on, the PAMP approach was also applied successfully to multi-objective design of lightweight thermoelastic structures [9] and multi-scale design of structures with maximum fundamental frequencies. Recently, Andreasen and Sigmund [10] suggested a multi-scale topology optimization method to design poroelastic actuators. We also refer the readers to [11–14] for more successful applications of multi-scale optimization method in different fields.

Despite remarkable achievements have been made for multi-scale design and optimization, it is worth noting that all of the existing works are carried out in a deterministic setting. Uncertainty is, however, ubiquitous in practical engineering design applications. A lot of evidences show that solutions to optimization problems can exhibit remarkable sensitivity to parameter perturbations. Recent years have also witnessed a growing research interest in the study of structural optimization problems considering uncertainties [15–23]. As for the multi-scale optimization problems considered in the present work, it can be expected that more attention should be paid to address the issue of uncertainties. This is because, on the one hand, compared with the fabrication of single scale macroscopic structures, there is higher probability to introduce manufacturing error when multi-scale structures are fabricated. On the other hand, since the minimum length scale of a multi-scale structure is usually very small (μm–mm), it will be much more sensitive to the unavoidable uncertainties. Therefore it is very necessary to take uncertainties into consideration in multi-scale optimization models otherwise the reliability of a multi-scale optimal design cannot be guaranteed. The present work is just a first attempt along this direction. In our study, we intend to develop a confidence multi-scale robust optimization model and the corresponding numerical solution approach considering unknown-but-bounded load uncertainties. The rest of the paper is organized as follows. Section 2 focuses on the mathematical formulation of the considered problem. In Section 3, numerical solution aspects including finite element discretization, confidence reformulation of the worst case scenario finding problem and sensitivity analysis are discussed. Two numerical examples are presented in Section 4 for demonstrating the effectiveness of the proposed problem formulation and the numerical solution approach. Finally, some concluding remarks are presented in Section 5.

2. Problem formulation

2.1. Problem statement

The robust optimization problem considered in the present work is to find the material distribution in the micro and macro scales concurrently with the aim of minimizing the worst case structural compliance under available material volume constraint. In order to make the solution process computationally tractable, the so called PAMP multi-scale optimization model proposed in [8], where the microstructure at every material point of a macro-scale structure is assumed to have the same form, is adopted to describe the material distribution in micro-scale and macro-scale, respectively (see Fig. 1 for a schematic illustration). Furthermore, the uncertainty of the external load is described by the classic ellipsoid model, which will be explained in more detail in Section 3.
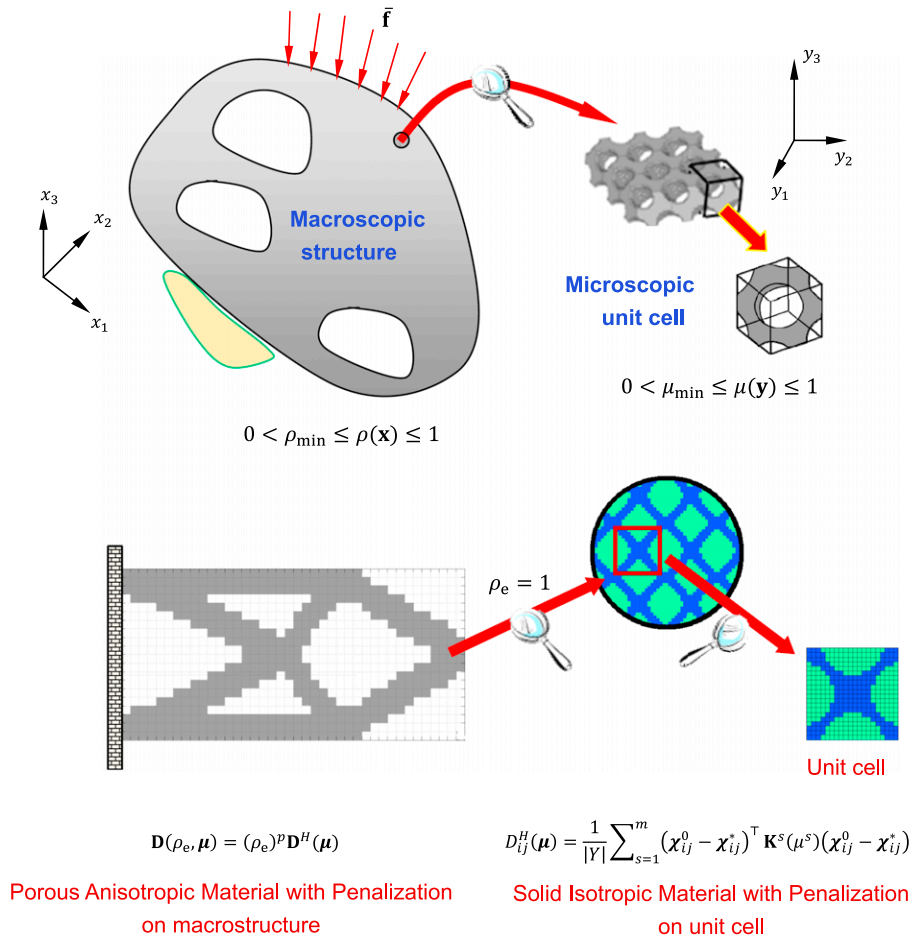
$$\mathbf{D}(\rho_e, \boldsymbol{\mu}) = (\rho_e)^p \mathbf{D}^H(\boldsymbol{\mu})$$

$$D_{ij}^H(\boldsymbol{\mu}) = \frac{1}{|Y|} \sum_{s=1}^{m} \left(\boldsymbol{\chi}_{ij}^0 - \boldsymbol{\chi}_{ij}^*\right)^\top \mathbf{K}^s(\mu^s)\left(\boldsymbol{\chi}_{ij}^0 - \boldsymbol{\chi}_{ij}^*\right)$$

Porous Anisotropic Material with Penalization on macrostructure

Solid Isotropic Material with Penalization on unit cell

Fig. 1. Schematic illustration of the PAMP multi-scale optimization model.

2.2. Mathematical formulation

The optimization problem described above can be formulated in the following form mathematically:

$\wp_U$

find $\rho(\mathbf{x}) \in L^\infty(D), \quad \mu(\mathbf{y}) \in L^\infty(Y)$

min $C_{\rho,\mu}$

s.t.

$$\frac{1}{|D|} \int_D \rho_0 \rho(\mathbf{x}) \mathrm{d}V \le \varsigma, \quad 0 < \rho_{\min} \le \rho(\mathbf{x}) \le 1,$$

$$\frac{1}{|Y|} \int_Y \mu(\mathbf{y}) \mathrm{d}Y = \rho_0, \quad 0 < \mu_{\min} \le \mu(\mathbf{y}) \le 1, \tag{2.1}$$

where $C_{\rho,\mu}$ is the *global optimal value* of the following maximization problem

$\wp_L(\rho, \mu)$

find $\bar{\mathbf{f}} \in U_{\bar{\mathbf{f}}}, \quad \mathbf{u}(\mathbf{x}) \in \left[\mathbf{H}^1(D)\right]^3$

max $l = \int_{S_t} \bar{\mathbf{f}} \cdot \mathbf{u} \mathrm{d}S$

s.t.

$$\int_D [\rho(\mathbf{x})]^p \, \mathbb{E}^H : \nabla \mathbf{u} : \nabla \mathbf{v} \mathrm{d}V = \int_{S_t} \bar{\mathbf{f}} \cdot \mathbf{v} \mathrm{d}S, \quad \forall \mathbf{v} \in U_{\mathrm{ad}},$$

$$\mathbf{u} = \bar{\mathbf{u}}, \quad \text{on } S_u, \tag{2.2}$$

with

$$\mathbb{E}^H : \nabla \mathbf{u} : \nabla \mathbf{u} = \min_{\chi - Y_{\mathrm{per}}} \frac{1}{|Y|} \int_Y [\mu(\mathbf{y})]^p \, \mathbb{E}^0 : \nabla \left(\mathbf{u} - \chi^* \right) : \nabla \left(\mathbf{u} - \chi^* \right) \mathrm{d}Y. \tag{2.3}$$

In Eq. (2.1), D and Y denote the macro-scale design domain and the unit cell on micro-scale, respectively. $\rho(\mathbf{x})$ and $\mu(\mathbf{y})$ are the artificial density fields depicting the material distributions in D and Y, respectively. ρ_0 denotes the porosity of the porous material used for constituting the macroscopic structure and ς denotes the upper bound of the volume fraction of the available solid material, respectively. Y_{per} is the function space χ belongs to and $Y_{\mathrm{per}} = \{ \chi | \chi \in \mathbf{H}^1(Y), \chi \text{ is periodic on } \partial Y \}$. The symbol χ^* in Eq. (2.3) is the character displacement field, which is periodic on ∂Y and $\mathbb{E}^H$ is the homogenized elasticity tensor of the porous material. $\mathbb{E}^0$ is the fourth order elasticity tensor of the solid material. S_u and S_t are the displacement prescribed and traction prescribed boundary of the macro-scale structure, respectively. $\bar{\mathbf{u}}$ and $\bar{\mathbf{f}}$ are the prescribed displacement and prescribed traction force on S_u and S_t, respectively. U_{ad} and $U_{\bar{\mathbf{f}}}$ represent the admissible set of the test functions (i.e., $\mathbf{v}$) and the uncertainty set of $\bar{\mathbf{f}}$, respectively. $\rho_{\min}$ and $\mu_{\min}$ are the lower bound of ρ and μ, respectively. In Eqs. (2.2) and (2.3), p is a penalization parameter introduced to suppress the intermediate density values implicitly.

It is worth noting that the above robust optimization problem is essentially a Bi-level program. That is in the upper level program $\wp_U$, one needs to find the optimal distributions of $\rho(\mathbf{x})$ and $\mu(\mathbf{y})$ under prescribed porosity and available material volume constraints. In order to get the value of the objective function (i.e. the worst case structural compliance), however, one must solve another mathematical program $\wp_L(\rho, \mu)$ (in which ρ and μ act as parameters) to find the worst case load scenario and the corresponding displacement field within $U_{\bar{\mathbf{f}}} \in \left[\mathbf{H}^1(D) \right]^3$, respectively. At this position, it is also necessary to emphasize that the lower level program $\wp_L(\rho, \mu)$ must be solved with global optimality otherwise the robustness of a structure cannot be evaluated accurately. This is because from theoretical point of view, only the global optimal value of $\wp_L(\rho, \mu)$ can represent the *worst case* structural compliance. It is, however, very difficult to obtain the global optimal solution of $\wp_L(\rho, \mu)$ since it is a non-convex (in fact an anti-convex) optimization problem. Therefore some further mathematical treatments are needed to on the one hand ensure the reliability of the obtained solution and on the other hand make the corresponding solution process computationally tractable. We will come back to this issue in Section 3.

3. Numerical solution aspects

3.1. Discrete problem formulation

In the present work, finite element method (FEM) is utilized to discretize the problem described in Eqs. (2.1)–(2.3). In both the macroscopic design domain D and the microscopic unit cell Y, the corresponding artificial density fields $\rho(\mathbf{x})$ and $\mu(\mathbf{y})$ are all interpolated by piecewise constant functions, that is

$$\rho(\mathbf{x}) = \rho_i, \quad \forall \mathbf{x} \in \Omega_i, \qquad \mu(\mathbf{y}) = \mu_j, \quad \forall \mathbf{y} \in \omega_j, \tag{3.1}$$

where $\bigcup_i \Omega_i = D$, $\Omega_i \cap \Omega_j = \emptyset$, $\forall i \neq j$ and $\bigcup_j \omega_j = Y$, $\omega_j \cap \omega_k = \emptyset$, $\forall j \neq k$, respectively. Under the aforementioned FEM discretization, the discrete form of the problem formulation can be written as

$$\tilde{\wp}_U$$

find $\boldsymbol{\rho} = (\rho_1, \ldots, \rho_n)^\top \in \mathbb{R}^n, \boldsymbol{\mu} = (\mu_1, \ldots, \mu_m)^\top \in \mathbb{R}^m$

min $C_{\rho, \mu}$

s.t.

$$\sum_{i=1}^n \rho_0 \rho_i \leq \zeta |D|, \qquad \sum_{j=1}^m \gamma_j = \rho_0 |Y|,$$

$$0 < \rho_{\min} \le \rho_i \le 1, \quad i = 1, \ldots, n,$$
$$0 < \mu_{\min} \le \mu_j \le 1, \quad j = 1, \ldots, m, \tag{3.2}$$

where $C_{\rho,\mu}$ is the *global optimal value* of the following maximization problem

$$\tilde{\wp}_L$$
find $\bar{\mathbf{t}} \in \mathbb{R}^l$
$$\max l = \bar{\mathbf{t}}^\top \mathbf{H}^\top \mathbf{K}^{-1}(\boldsymbol{\rho}, \boldsymbol{\mu}) \mathbf{H} \bar{\mathbf{t}}$$
s.t. $\bar{\mathbf{t}} \in U_{\bar{\mathbf{t}}}$, \tag{3.3}

where

$$\mathbf{K}(\boldsymbol{\rho}, \boldsymbol{\mu}) = \sum_{e=1}^n (\rho_e)^p \int_{V^e} \mathbf{B}^\top \mathbf{D}^H(\boldsymbol{\mu}) \mathbf{B} \mathrm{d} V^e \tag{3.4a}$$

and

$$D_{ij}^H(\boldsymbol{\mu}) = \frac{1}{|Y|} \sum_{s=1}^m \left(\boldsymbol{\chi}_{ij}^0 - \boldsymbol{\chi}_{ij}^* \right)^\top \mathbf{K}^s(\mu^s) \left(\boldsymbol{\chi}_{ij}^0 - \boldsymbol{\chi}_{ij}^* \right), \quad i, j = 1, 2, 3. \tag{3.4b}$$

In Eq. (3.2), n and m denote the total number of finite elements used for discretizing the macroscopic design domain D and the unit cell Y, respectively. $\mathbf{H}$ is an aggregation matrix which generates the load vector $\bar{\mathbf{f}}$ from its non-zero components $\bar{\mathbf{t}}$ such that $\bar{\mathbf{f}} = \mathbf{H}\bar{\mathbf{t}}$ [24]. In Eq. (3.4a), $\mathbf{B}$ is the strain matrix. $\mathbf{K}(\boldsymbol{\rho}, \boldsymbol{\mu})$ is the global stiffness matrix corresponding to the FEM discretization of D while $\mathbf{D}^H(\boldsymbol{\mu})$ is the homogenized elastic matrix of the porous material whose components can be obtained by summing up the strain energies on the unit cell as shown in Eq. (3.4b). In Eq. (3.4b), $\mathbf{K}^s(\mu^s) = (\mu^s)^p \int_Y \mathbf{B}^\top \mathbf{D}^0 \mathbf{B} \mathrm{d} Y$ is the stiffness matrix of the sth element in Y where $\mathbf{B}$ and $\mathbf{D}^0$ are the strain matrix and the elasticity matrix corresponding to the solid material, respectively. μ^s is the artificial density of the sth element in the microscopic unit cell. The symbols $\boldsymbol{\chi}_{ij}^0$ as well as $\boldsymbol{\chi}_{ij}^*$, $i, j = 1, 2, 3$ denote the displacement vectors associated with the unit initial strains and the corresponding characteristic displacement vectors on Y, respectively. We refer the readers to [25] for more details on the FEM implementation of the asymptotic homogenization theory.

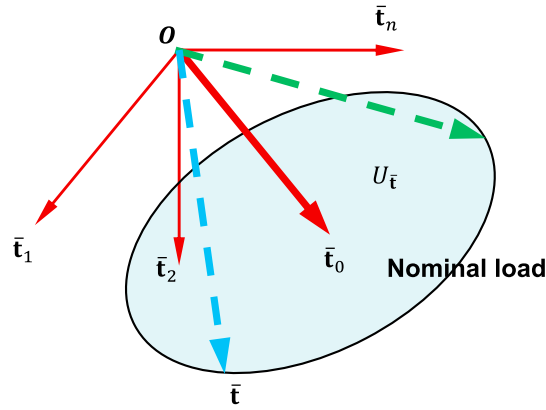### 3.2. Uncertain set of the external load

In the present work, the uncertainty of the external loads is described by the following ellipsoid model

$$U_{\bar{\mathbf{t}}} = \left\{ \bar{\mathbf{t}} \mid (\bar{\mathbf{t}} - \bar{\mathbf{t}}_0)^\top \bar{\mathbf{B}}_i (\bar{\mathbf{t}} - \bar{\mathbf{t}}_0) - 1 \le 0, \ i = 1, \ldots, s \right\}, \tag{3.5}$$

where $\bar{\mathbf{t}}_0$ is the nominal aggregated load vector generated by the nominal non-zero components of $\bar{\mathbf{f}}$ (external load vector) and $\bar{\mathbf{B}}_i$, $i = 1, \ldots, s$ are the shape matrices which represent the correlations between the individual components of $\bar{\mathbf{t}}$ (see Fig. 2 for reference). As pointed in many references [17,18], ellipsoid model is a very powerful tool to describe the unknown-but-bounded uncertainties especially when the exact probability information of the uncertainty is not available. Compared with the interval model, it also has the advantage of being capable of describing the correlations between different uncertain variables.

3.3. Confidence reformulation of the lower level program

As pointed in the previous section, it is very necessary to obtain the global optima of the lower level programs in Eqs. (2.2) and (3.3) in order to evaluate the worst case structural compliance accurately (see Fig. 3 for a schematic illustration). However, a careful observation of the inner program in Eq. (3.3) indicates that it is in fact an anti-convex program (*maximization* of a quadratic function on a convex set) where many local optima may exist in the feasible set. Under this circumstance, it is highly possible that the numerical solution algorithm of $\tilde{\wp}_L$ will get stuck at a local optimum and therefore underestimates the worst case structural compliance severely. This means that if one solves $\tilde{\wp}_L$ directly, the reliability of the optimal solution thus obtained cannot be fully assured at least theoretically. It is also worth noting that in fact the Bi-level program in Eqs. (3.2) and (3.3) is very difficult to deal with. As pointed out by

$$U_{\bar{\mathbf{t}}} = \{\bar{\mathbf{t}}|(\bar{\mathbf{t}} - \bar{\mathbf{t}}_0)^\top \bar{\mathbf{B}}(\bar{\mathbf{t}} - \bar{\mathbf{t}}_0) - 1 \le 0\}$$

Fig. 2. Uncertainty description of the external load.

● True worst-case response (global maximum)
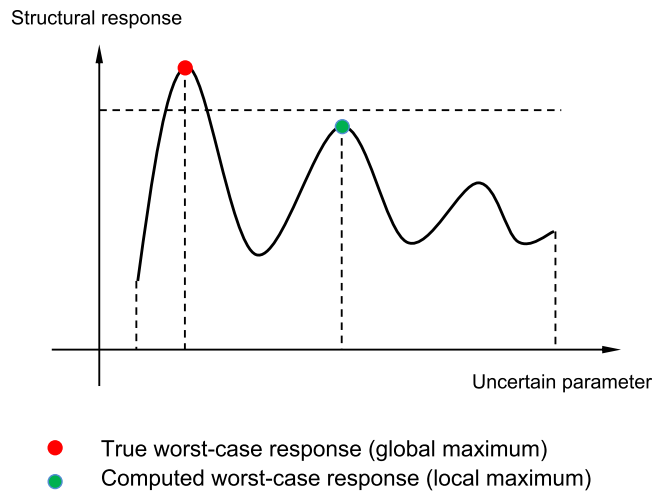● Computed worst-case response (local maximum)

Fig. 3. Local optimum and global optimum in robust optimization. If the concerned function is a non-convex function of the uncertain parameters, the computed worst-case structural response (local maximum) may underestimate the true worst-case structural response (global maximum) severely.

Dempe and Dutta [26], for a general Bi-level program (it is not difficult to prove that $\tilde{\wp}_L$ does can be transformed to the following form equivalently)

$$\begin{cases} \min_{\mathbf{x},\mathbf{y}} \{F(\mathbf{x}, \mathbf{y}) : \mathbf{x} \in X, \, \mathbf{y} \in \phi(\mathbf{x}) \cap Y\}, \\ \mathbf{y} \in \phi(\mathbf{x}) := \operatorname{Arg\,min}_{\mathbf{y}} \{f(\mathbf{x}, \mathbf{y}) : \, \mathbf{g}(\mathbf{x}, \mathbf{y}) \le \mathbf{0}\}, \end{cases} \tag{3.6}$$

only when the lower level program is convex with respect to $\mathbf{y}$ for every fixed $\mathbf{x}$ and some regularity conditions are satisfied, the equivalence between the global optimal solution of Eq. (3.6) and that of a single level program can be established. If the convexity requirement of the lower level program cannot be satisfied, it is even impossible to establish the conditions characterizing the critical points of Eq. (3.6). Furthermore, if the lower level program is not convex, the computation efforts associated with solving the Bi-level program may be very large. We refer the readers to [21] for more discussions and examples on the necessity of constructing confidence formulations for robust optimization.

Based on the above discussions, in the following, we will employ the method developed in [21] to construct a confidence reformulation of $\tilde{\wp}_L$ in Eq. (3.3) with use of the so-called Semi-Definite Programming (SDP) relaxation

technique [27]. The essential idea is that instead of tackling the *non-convex* lower level program $\tilde{\wp}_L$ directly, a conservative *convex* program $\hat{\wp}_L$, whose global optimal value is a strict upper bound of the global optimal value of $\tilde{\wp}_L$, is solved. This can be achieved by constructing the dual problem of $\tilde{\wp}_L$. Following the same steps as in [21], $\hat{\wp}_L$, which is a linear SDP problem, can be written as

$$
\begin{aligned}
&\hat{\wp}_L \\
&\text{find } t \in \mathbb{R}, \quad \boldsymbol{\lambda} = (\lambda_1, \ldots, \lambda_s)^\top \in \mathbb{R}_+^p \\
&\min t \\
&\text{s.t.} \\
&\mathbf{G} = \begin{bmatrix} -\bar{\mathbf{M}} + \sum_{i=1}^s \lambda_i \bar{\mathbf{B}}_i & -\sum_{i=1}^s \lambda_i \bar{\mathbf{B}}_i \bar{\mathbf{t}}_0 \\ \text{sym.} & \sum_{i=1}^s \lambda_i (\bar{\mathbf{t}}_0^\top \bar{\mathbf{B}}_i \bar{\mathbf{t}}_0 - 1) + t \end{bmatrix} \succeq \mathbf{0}, \\
&\lambda_i \geq 0, \quad i = 1, \ldots, s,
\end{aligned}
\tag{3.7}
$$

with $\bar{\mathbf{M}} = \mathbf{H}^\top \mathbf{K}^{-1} \mathbf{H}$.

If $t = \tilde{C}_{\rho,\mu}$ is the global optimal value of $\hat{\wp}_L$ and $l = C_{\rho,\mu}$ is the global optimal value of $\tilde{\wp}_L$, then from the theorem of weak duality in convex analysis [27], the following inequality:

$$
C_{\rho,\mu} \leq \tilde{C}_{\rho,\mu},
\tag{3.8}
$$

always holds. This means that $\tilde{C}_{\rho,\mu}$ is always a conservative estimation of the worst case structural compliance. Furthermore, based on the strong duality theorem [27], there is in fact no dual gap (i.e., $C_{\rho,\mu} = \tilde{C}_{\rho,\mu}$) between $\tilde{\wp}_L$ and $\hat{\wp}_L$ if there is only one ellipsoid (i.e. $s = 1$). It is also worth noting that $\hat{\wp}_L$ is a convex SDP problem which can be solved very efficiently by modern interior point algorithms. This is very helpful for alleviating the computational burden in solving the Bi-level optimization problem. We refer the readers to [21] for more discussions on this aspect.

3.4. Sensitivity analysis

In order to solve the Bi-level program in Eqs. (3.2) and (3.3) with use of gradient-based optimization algorithms, we need the sensitivities of $\tilde{C}_{\rho,\mu}$ with respect to $\rho(\mathbf{x})$ and $\mu(\mathbf{y})$. As discussed in [28], under some regularity conditions, these quantities can be obtained by the perturbation analysis of a linear SDP problem with respect to its parameters. Denoting

$$
\tilde{C}_{\rho,\mu} = \min_{t \in \mathbb{R}, \boldsymbol{\lambda} \geq \mathbf{0}} \{t | \mathbf{G}(t, \boldsymbol{\lambda}; \boldsymbol{\rho}, \boldsymbol{\mu}) \succeq \mathbf{0}\},
\tag{3.9}
$$

where

$$
\mathbf{G}(t, \boldsymbol{\lambda}; \boldsymbol{\rho}, \boldsymbol{\mu}) = \begin{bmatrix} -\bar{\mathbf{M}} + \sum_{i=1}^s \lambda_i \bar{\mathbf{B}}_i & -\sum_{i=1}^s \lambda_i \bar{\mathbf{B}}_i \bar{\mathbf{t}}_0 \\ \text{sym.} & \sum_{i=1}^s \lambda_i \left(\bar{\mathbf{t}}_0^\top \bar{\mathbf{B}}_i \bar{\mathbf{t}}_0 - 1 \right) + t \end{bmatrix},
\tag{3.10}
$$

then according to the theoretical results obtained in [28] (assuming that required regularity conditions are satisfied), we have

$$
\frac{\partial \tilde{C}_{\rho,\mu}(\boldsymbol{\rho}, \boldsymbol{\gamma})}{\partial \rho_i} = \frac{\partial L(t^*, \boldsymbol{\lambda}^*, \mathbf{Y}^*; \boldsymbol{\rho}, \boldsymbol{\mu})}{\partial \rho_i} = \text{trace}\left(\mathbf{Y}^{*\top} \mathbf{G}_{\rho_i}\right),
\tag{3.11}
$$

$$
\frac{\partial \tilde{C}_{\rho,\mu}(\boldsymbol{\rho}, \boldsymbol{\gamma})}{\partial \mu_j} = \frac{\partial L(t^*, \boldsymbol{\lambda}^*, \mathbf{Y}^*; \boldsymbol{\rho}, \boldsymbol{\mu})}{\partial \mu_j} = \text{trace}\left(\mathbf{Y}^{*\top} \mathbf{G}_{\mu_j}\right),
\tag{3.12}
$$

where

$$L = L\left(t, \lambda, \mathbf{Y}; \boldsymbol{\rho}, \boldsymbol{\mu}\right) = t - \mathbf{Y} \cdot \mathbf{G}(t, \lambda; \boldsymbol{\rho}, \boldsymbol{\mu}) + \Sigma^\top \left(-\lambda\right), \tag{3.13a}$$

$$\mathbf{G}_{\rho_i} = \frac{\partial \mathbf{G}}{\partial \rho_i} = - \begin{bmatrix} \dfrac{\partial \bar{\mathbf{M}}}{\partial \rho_i} & \mathbf{0} \\[2mm] \mathbf{0} & 0 \end{bmatrix} \tag{3.13b}$$

and

$$\mathbf{G}_{\mu_j} = \frac{\partial \mathbf{G}}{\partial \mu_j} = - \begin{bmatrix} \dfrac{\partial \bar{\mathbf{M}}}{\partial \mu_j} & \mathbf{0} \\[2mm] \mathbf{0} & 0 \end{bmatrix}, \tag{3.13c}$$

respectively. In Eqs. (3.11), (3.12) and (3.13a), L is the Lagrange function of $\hat{\wp}_L$ and $\mathbf{Y}$ as well as Σ are the corresponding Lagrange multipliers associated with the constraint functions $\mathbf{G}(t, \lambda; \boldsymbol{\rho}, \boldsymbol{\mu}) \succcurlyeq \mathbf{0}$ and $\lambda \geq \mathbf{0}$, respectively. t^*, λ^* and $\mathbf{Y}^*$ are the optimal values of the primal and dual variables ($\boldsymbol{\rho}$ and $\boldsymbol{\mu}$ are fixed) associated with $\hat{\wp}_L$, respectively.

The values of $\partial \bar{\mathbf{M}}/\partial \rho_i$ and $\partial \bar{\mathbf{M}}/\partial \mu_j$ in Eqs. (3.13b) and (3.13c) can be obtained as follows.

Let $\mathbf{Z} \in \mathbb{R}^{n^d \times n^m}$ (here n^d is the dimension of $\bar{\mathbf{f}}$ and n^m is the number of the non-zero components of $\bar{\mathbf{f}}$, respectively) is the solution of the following matrix equation

$$\mathbf{K}\mathbf{Z} = \mathbf{H}, \tag{3.14}$$

where $\mathbf{K} \in \mathbb{R}^{n^d \times n^d}$ and $\mathbf{H} \in \mathbb{R}^{n^d \times n^m}$, respectively. Then we have

$$\bar{\mathbf{M}} = \mathbf{Z}^\top \mathbf{K} \mathbf{Z}. \tag{3.15}$$

In light of Eq. (3.15), it yields that

$$\frac{\partial \bar{\mathbf{M}}}{\partial \rho_i} = \frac{\partial \left(\mathbf{Z}^\top \mathbf{K} \mathbf{Z}\right)}{\partial \rho_i} = \frac{\partial \mathbf{Z}^\top}{\partial \rho_i} \mathbf{K} \mathbf{Z} + \mathbf{Z}^\top \frac{\partial \mathbf{K}}{\partial \rho_i} \mathbf{Z} + \mathbf{Z}^\top \mathbf{K} \frac{\partial \mathbf{Z}}{\partial \rho_i}. \tag{3.16}$$

From Eq. (3.14), the following relationship holds (note that $\partial \mathbf{H}/\partial \rho_i = \mathbf{0}$)

$$\frac{\partial \mathbf{K}}{\partial \rho_i} \mathbf{Z} + \mathbf{K} \frac{\partial \mathbf{Z}}{\partial \rho_i} = \mathbf{0}, \tag{3.17}$$

which implies that

$$\mathbf{Z}^\top \frac{\partial \mathbf{K}}{\partial \rho_i} \mathbf{Z} + \mathbf{Z}^\top \mathbf{K} \frac{\partial \mathbf{Z}}{\partial \rho_i} = \mathbf{0} \tag{3.18a}$$

and

$$\frac{\partial \mathbf{Z}^\top}{\partial \rho_i} \mathbf{K} \mathbf{Z} = -\mathbf{Z}^\top \frac{\partial \mathbf{K}}{\partial \rho_i} \mathbf{Z}. \tag{3.18b}$$

Since

$$\mathbf{K}(\boldsymbol{\rho}, \boldsymbol{\mu}) = \sum_{j=1}^{n} \left(\rho_j\right)^p \int_{V^j} \mathbf{B}^\top \mathbf{D}^H(\boldsymbol{\mu}) \mathbf{B} \mathrm{d}V^j,$$

we finally arrive at the result that

$$\frac{\partial \bar{\mathbf{M}}}{\partial \rho_i} = -\mathbf{Z}^\top \left(p \, (\rho_i)^{p-1} \int_{V^i} \mathbf{B}^\top \mathbf{D}^H(\boldsymbol{\mu}) \mathbf{B} \mathrm{d} V^i \right) \mathbf{Z}. \tag{3.19}$$

Similarly, we also have

$$\frac{\partial \bar{\mathbf{M}}}{\partial \mu_j} = -\mathbf{Z}^\top \left(\sum_{j=1}^{n} (\rho_j)^p \int_{V^j} \mathbf{B}^\top \frac{\partial \mathbf{D}^H(\boldsymbol{\mu})}{\partial \mu_j} \mathbf{B} \mathrm{d} V^j \right) \mathbf{Z}, \tag{3.20}$$

where

$$\frac{\partial D_{kl}^H(\boldsymbol{\mu})}{\partial \mu_j} = \frac{1}{|Y|} p \left(\chi_{kl}^0 - \chi_{kl}^* \right)^\top (\mu_j)^{p-1} \mathbf{K}^{0j} \left(\chi_{kl}^0 - \chi_{kl}^* \right), \quad k, l = 1, 2, 3 \tag{3.21}$$

with $\mathbf{K}^{0j}$ denoting the element stiffness matrix of the jth element in Y when $\mu_j = 1$.

3.5. Sensitivity filter

It is well known that in SIMP (Solid Isotropic Material with Penalization) based topology optimization framework, regularization schemes are needed to obtain mesh-independent results. Among numerous approaches proposed to suppress the numerical instabilities in topology optimization, the sensitivity filter approach proposed by Sigmund [29] is the most efficient one. The original form of the sensitivity filter scheme can be written as

$$\frac{\widehat{\partial l}}{\partial \rho_k} = \frac{1}{\rho_k \sum\limits_{i=1}^{N} \hat{H}_i} \sum_{i=1}^{N} \hat{H}_i \rho_i \frac{\partial l}{\partial \rho_i}, \tag{3.22}$$

where $\widehat{\partial l}/\partial \rho_k$ and $\partial l/\partial \rho_i$ are the filtered and unfiltered sensitivities of the concerned objective/constraint functional l (for the considered problem, l is the structural compliance). The symbols ρ_k and ρ_i denote the densities of the considered kth element and the ith element contained in the filter region of element k. N is the total number of elements in the spherical filter region with radius R. The weight factor $\hat{H}_i$ are defined as

$$\hat{H}_i = R - \mathrm{dist}(i, k), \quad \forall i \text{ such that dist } (i, k) \leq R \tag{3.23}$$

where $\mathrm{dist}(i, k)$ is the distance between the centers of element i and k. Although powerful enough, an unpleasant behavior of the filter scheme in Eq. (3.22) is that it will inevitably lead to the so-called boundary diffusion effect, i.e., appearance of gray elements along the structural boundary. In order to alleviate the boundary diffusion effect associated with the filter scheme in Eq. (3.22), here, we adopt a modified filter scheme [30], which can be expressed in the following form:

$$\frac{\widetilde{\partial l}}{\partial \rho_k} = \frac{1}{(\rho_k)^\eta + \left(\sum\limits_{j=1}^{4} \rho_j \right)^\nu} \frac{\sum\limits_{i=1}^{N} \hat{H}_i \, (\rho_i)^\gamma \, \frac{\partial l}{\partial \rho_i}}{\sum\limits_{i=1}^{N} \hat{H}_i}, \tag{3.24}$$

where $0 < \eta < 1$, $\gamma \geq 1$ and $0 < \nu < 1$ are three adjustable parameters. In Eq. (3.24), the summation in $\sum_{j=1}^{4} \rho_j$ is taken for the four second-nearest neighborhood elements around element k. The basic mechanism of this modified filter scheme responsible for alleviating the boundary diffusion effect is to appropriately reduce the value of the sensitivity with respect to ρ_k that takes small value in a non-checkerboard distribution of ρ. We refer the readers to Fig. 4 and [30] for a schematic illustration and the demonstration of the effectiveness of this treatment. Numerical experiments in Section 4 show that the above filter scheme is very effective to eliminate gray elements along the structural boundary and therefore is helpful for obtaining nearly black-and-white designs.
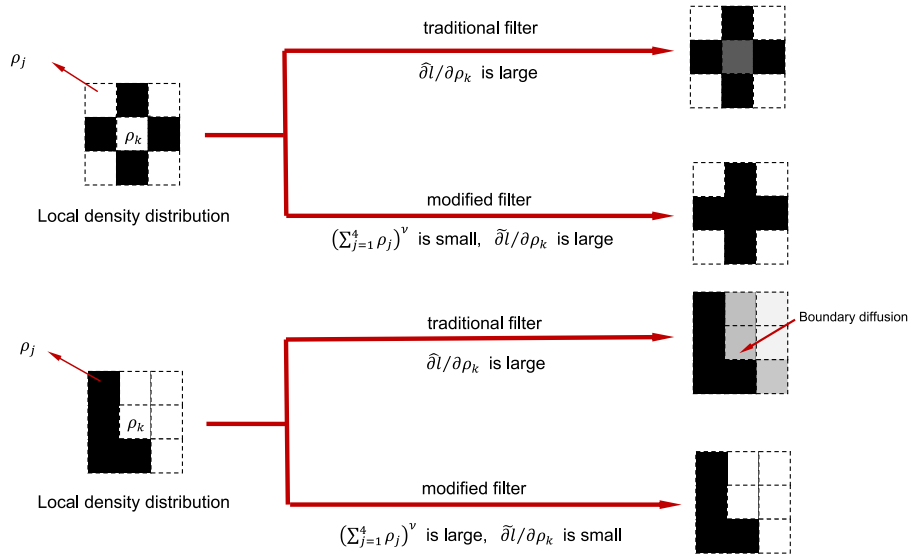
Fig. 4. A schematic illustration of the proposed modified filter approach.

3.6. Solution scheme

Based on the above analysis, the solution procedure of the considered multi-scale robust optimization problem can be summarized as follows:

(1) Set $k = 0$ and initialize the design variables $\rho(\mathbf{x}) = \rho^0(\mathbf{x})$ and $\mu(\mathbf{y}) = \mu^0(\mathbf{y})$ respectively;

(2) Compute the homogenized elastic matrix $\mathbf{D}^H$ based on $\mu^k(\mathbf{y})$;

(3) For $\rho(\mathbf{x}) = \rho^k(\mathbf{x})$ and $\mu(\mathbf{y}) = \mu^k(\mathbf{y})$, solve the lower level SDP problem and get $\tilde{C}_{\rho^k,\mu^k}$ and $\partial\tilde{C}_{\rho^k,\mu^k}/\partial\boldsymbol{\rho}$ as well as $\partial\tilde{C}_{\rho^k,\mu^k}/\partial\boldsymbol{\mu}$, respectively;

(4) Solve the upper level optimization with use of gradient-based optimization algorithm (e.g., MMA (Method of Moving Asymptotes) [31]) and update $\rho^k(\mathbf{x})$ and $\mu^k(\mathbf{y})$, respectively;

(5) Check convergence, If converged then stop; otherwise set $k = k + 1$, $\rho^k(\mathbf{x}) \Rightarrow \rho^{k+1}(\mathbf{x})$, $\mu^k(\mathbf{y}) \Rightarrow \mu^{k+1}(\mathbf{y})$ and go to step 2.

The above solution procedure is illustrated in the flow chart shown in Fig. 5.

4. Numerical examples

In this section, the proposed approach is applied to several two dimensional (with unit thickness) plane stress examples to illustrate its effectiveness. All involved quantities are dimensionless for the sake of simplicity. In all examples, the macroscopic design domains and the microscopic unit cells are discretized by uniform four-node bilinear square elements, which is a popular choice for topology optimization and material design problems. The Young's modulus and the Poisson's ratio of the isotropic solid material are chosen as $E = 10$ and $\nu = 0.3$, respectively. The filter radius is set to be 1.2 for sensitivities with respect to both microscopic and macroscopic design variables. In all example, we take $\rho_{\min} = 1.0e{-}03$, $\mu_{\min} = 1.0e{-}03$ and $p = 3$, respectively and the values of the parameters η, ν and γ in the modified filter scheme are chosen as 0.1, 0.05 and 2, respectively, based on our numerical experiences. Furthermore, the upper level optimization problems in Eq. (3.2) are solved by the MMA algorithm while the lower level linear SDP problems in Eq. (3.7) are solved by SDPA [32], a reliable LSDP solver.

In all numerical examples, the initial values of the macroscopic design variables are all taken as $\rho^0 = 0.5$. In contrast, we take the non-uniform design shown in Fig. 6 as the starting point for microscopic topology optimization since it is well known that uniform initial design cannot be used to solve material design problems [33].
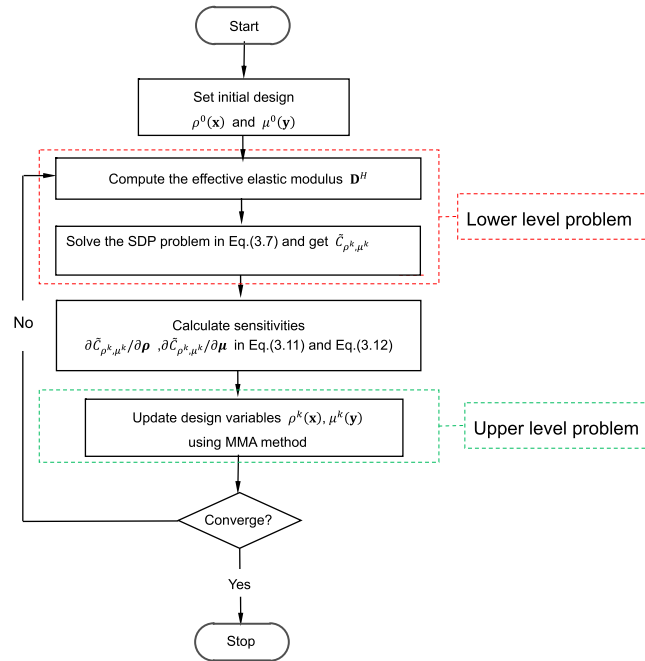
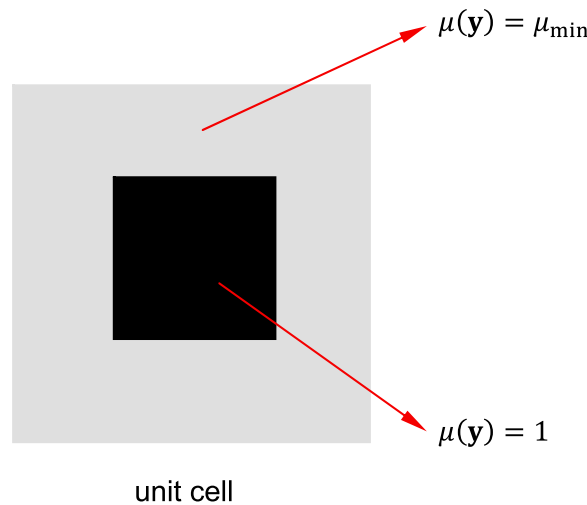Fig. 5. The flow chart of the optimization procedure.

unit cell

Fig. 6. The initial design of the microscopic unit cell.

4.1. L-shape beam example

In this example, the classical L-shape beam problem shown in Fig. 7 is investigated. The finite element meshes are 40×40 for macroscopic design domain and 20×20 for microscopic unit cell, respectively. The upper bound of the volume ratio of the available solid material is $\varsigma = 0.12$ and the apparent density of the cellular material is $\rho_0 = 0.4$.

For comparison purpose, first, the example is examined with a deterministic nominal load $\bar{\mathbf{t}}_0 = (0, 0.5)^\top$ applied at the left-middle point of the design domain by applying the traditional and the modified filter scheme in Eq. (3.24), respectively. The optimal material distributions on different length scales are shown in Fig. 8(a) and (b), respectively. It can be observed from these figures that traditional filter scheme will lead to strong boundary diffusion effect while the result obtained under the modified filter scheme is almost black-and-white.
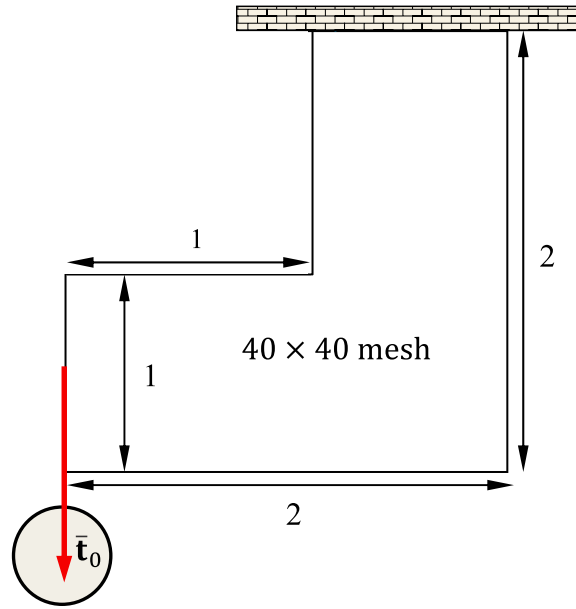
Fig. 7. The L-shape beam example.

Optimal material distributions under nominal load $\bar{\mathbf{t}}_0$

Optimal material distributions under uncertain load

Boundary diffusion
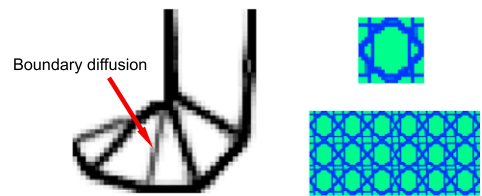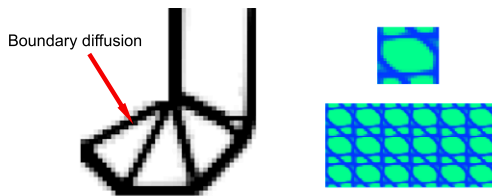
(a) traditional filter approach

Boundary diffusion

(c) traditional filter approach
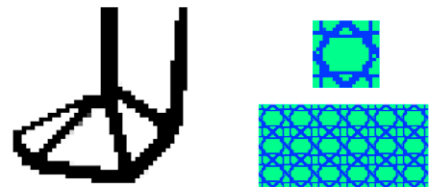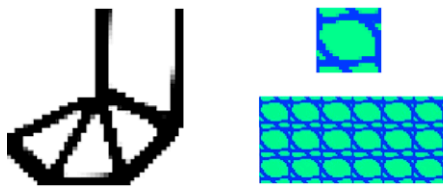
(b) modified filter approach

(d) modified filter approach

Fig. 8. Optimal material distributions of L-shape beam example.

Next, the same problem is solved with use of problem formulation Eq. (3.3) considering uncertain load, which can be described as $\left(\bar{\mathbf{t}} - \bar{\mathbf{t}}_0\right)^{\top} \bar{\mathbf{B}} \left(\bar{\mathbf{t}} - \bar{\mathbf{t}}_0\right) - 1 \leq 0$ with $\bar{\mathbf{B}} = \begin{bmatrix} 16 & 0 \\ 0 & 16 \end{bmatrix}$. The corresponding optimization results are shown in Fig. 8(c) and (d), respectively. It can be observed from Fig. 8 that compared with the deterministic optimal solution, considering the uncertainty of the external load will not change the macroscopic structure too much. The microscopic material distribution is, however, quite different in two cases. It seems that the form of microstructure is more sensitive to the load uncertainties than that of macrostructure for the problem considered. Numerical results also reveal that when cellular materials are available, it is more economic to resist the direction-variable uncertainty load
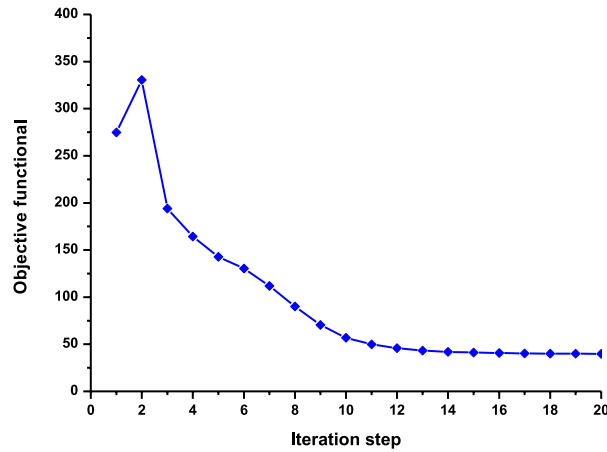
Fig. 9. The iteration history of the L-shaped beam example under uncertain load.
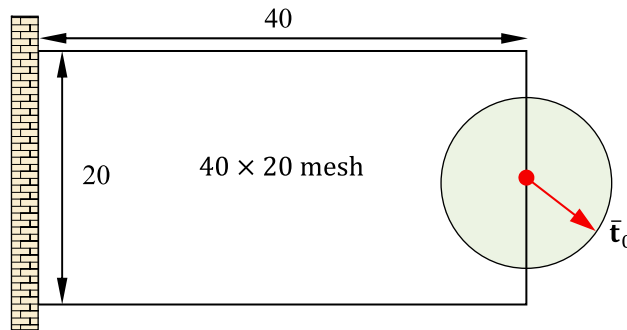
Fig. 10. The cantilever beam example.

by rendering a more isotropic (i.e., with higher structural symmetry) microscopic material distribution on micro-scale rather than changing the configuration of macrostructure, which determines the primary path of load transfer.

Fig. 8 also indicates that the difference between the optimal microscopic material distributions obtained under two cases is solely due to the consideration of load uncertainties, but not due to the adoption of modified filter approach.

The convergence history of this example is shown in Fig. 9. We can find that after a slight increase, the value of the objective function decreases dramatically within ten iteration steps and tends to be converged within another ten steps. This indicates a rapid convergence rate for this example.

4.2. Cantilever beam example

In this example, the cantilever beam problem shown in Fig. 10 is investigated. The macroscopic design domain and microscopic unit cell are discretized by a 40×20 mesh and a 20×20 mesh, respectively. The uncertain load applied at the right-middle point is described by $(\bar{\mathbf{t}} - \bar{\mathbf{t}}_0)^\top \bar{\mathbf{B}} (\bar{\mathbf{t}} - \bar{\mathbf{t}}_0) - 1 \leq 0$ with $\bar{\mathbf{t}}_0 = \mathbf{0}$ and $\bar{\mathbf{B}} = \begin{bmatrix} 1 & 0 \\ 0 & 1 \end{bmatrix}$. In this example, we intend to discuss the effect of the parameters ρ_0 and ς on the multi-scale optimal solutions. First, the considered problem is solved with fixed value of ρ_0 (i.e., $\rho_0 = 0.4$) but different values of ς (i.e., $\varsigma = 0.14$, $\varsigma = 0.16$, $\varsigma = 0.18$ and $\varsigma = 0.2$, respectively). The corresponding optimal material distributions are shown in Table 1. From this table, it is observed that the compliance of the optimal structure decreases as ς increases but the material distribution in the microscopic unit cell is almost the same (all are Kagome type microstructures) as ς varies. Next, optimizations are carried out under fixed value of ς (i.e., $\varsigma = 0.2$) but this time the values of ρ_0 are changed from 0.4 to 0.7. Under this circumstance, the corresponding optimal material distributions are shown in Table 2. From Table 2, it can be observed that as ρ_0 increases, the structural members in the microscopic unit cell become thicker while the structural members (composed by the cellular material with density ρ_0) in the macroscopic structure become thinner in order to satisfy the

Table 1
Numerical results under uncertain load (with fixed ρ_0).

ς	ρ_0	Compliance	Macro-scale structural topology	Micro-scale structural topology	
0.14	0.4	15.3024			
0.16	0.4	14.3120			
0.18	0.4	10.1428			
0.20	0.4	9.0691			

Table 2
Numerical results under uncertain load (with fixed ς).

ς	ρ_0	Compliance	Macro-scale structural topology	Micro-scale structural topology	
0.2	0.4	9.0691			
0.2	0.5	8.4658			
0.2	0.6	7.7189			
0.2	0.7	6.9431			

available solid material volume upper bound. As in the previous example, the Kagome like microstructure with near isotropic material distribution seems to be optimal to enhance the robustness of the structure under uncertain external loads. It is also very interesting to note that the resulting microstructure is similar to that of deep-sea sponges (shown in Fig. 11), which are created through millions years of natural evolution and very helpful to resist the forces induced by currents from different directions [34].

5. Concluding remarks

In the present paper, robust concurrent optimization of material and structure under unknown-but-bounded load uncertainties is investigated in a multi-scale framework. Problem formulation that can allow for the effect of worst-case
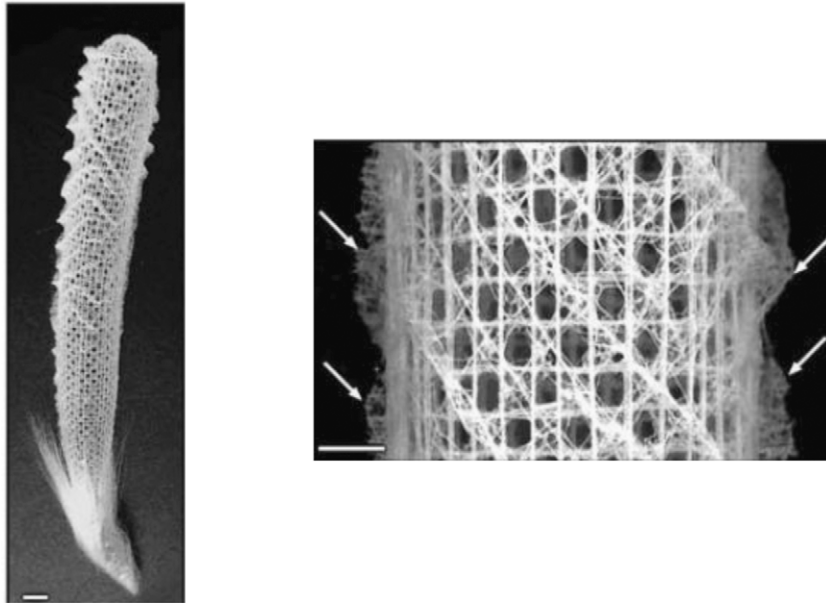
Fig. 11. Hierarchical structure of deep-sea sponge.
Source: From [34].

scenario in a confidence way and the corresponding numerical solution procedure are proposed. Numerical examples demonstrate that when load uncertainties are considered, optimal material distributions in microstructures tend to be isotropic and Kagome structure seems to be superior to other forms of microstructures. In the present work, only load uncertainty is considered. Considering material uncertainty, which is ubiquitous in practical engineering design applications and may be possibly induced by material degradation, accidental damage or manufacture error, in a multi-scale framework, however, is difficult since structural responses are usually implicit functions of material properties. This will pose great challenges to constructing the corresponding confidence robust formulation and developing the computationally tractable solution algorithms. We will pursue this issue in the future work.

Acknowledgments

References

[1] M.P. Bendsoe, N. Kikuchi, Generating optimal topologies in structural design using a homogenization method, Comput. Methods Appl. Mech. Engrg. 71 (1988) 197–224.
[2] H.A. Eschenauer, N. Olhoff, Topology optimization of continuum structures: a review, Appl. Mech. Rev. 54 (2001) 331–390.
[3] X. Guo, G.D. Cheng, Recent development in structural design and optimization, Acta Mech. Sin. 26 (2010) 807–823.
[4] O. Sigmund, K. Maute, Topology optimization approaches, Struct. Multidiscip. Optim. 48 (2013) 1031–1055.
[5] R. Lakes, Materials with structural hierarchy, Nature 361 (1993) 511–515.
[6] T.A. Schaedler, A.J. Jacobsen, A. Torrents, et al., Ultralight metallic microlattices, Science 334 (2011) 962–965.
[7] H. Rodrigues, J.M. Guedes, M.P. Bendsoe, Hierarchical optimization of material and structure, Struct. Multidiscip. Optim. 24 (2002) 1–10.
[8] L. Liu, J. Yan, G.D. Cheng, Optimum structure with homogeneous optimum truss-like material, Comput. Struct. 86 (2008) 1417–1425.
[9] J.D. Deng, J. Yan, G.D. Cheng, Multi-objective concurrent topology optimization of thermoelastic structures composed of homogeneous porous material, Struct. Multidiscip. Optim. 47 (2013) 583–597.
[10] C.S. Andreasen, O. Sigmund, Multiscale modeling and topology optimization of poroelastic actuators, Smart Mater. Struct. 21 (2012) 065005. 1–14.
[11] X. Yan, X. Huang, Y. Zha, Y.M. Xie, Concurrent topology optimization of structures and their composite microstructures, Comput. Struct. 133 (2014) 103–110.

[12] Z.H. Zuo, X.D. Huang, J.H. Rong, Y.M. Xie, Multi-scale design of composite materials and structures for maximum natural frequencies, Mater. Des. 51 (2013) 1023–1034.

[13] X. Huang, S.W. Zhou, Y.M. Xie, Q. Li, Topology optimization of microstructures of cellular materials and composites for macrostructures, Comput. Mater. Sci. 67 (2013) 397–407.

[14] Y.M. Xie, Z.H. Zuo, X.D. Huang, J.H. Rong, Convergence of topological patterns of optimal periodic structures under multiple scales, Struct. Multidiscip. Optim. 46 (2012) 41–50.

[15] C.P. Pantelides, S. Ganzerli, Design of trusses under uncertain loads using convex models, J. Struct. Engrg. 124 (1998) 318–329.

[16] M. Lombardi, R.T. Haftka, Anti-optimization techniques for structural design under load uncertainties, Comput. Methods Appl. Mech. Engrg. 157 (1998) 19–31.

[17] F.T.K. Au, Y.S. Cheng, L.G. Tham, G.W. Zeng, Robust design of structures using convex models, Comput. Struct. 81 (2003) 2611–2619.

[18] I. Elishakoff, R.T. Haftka, J. Fang, Structural design under bounded uncertainty optimization with anti-optimization, Comput. Struct. 53 (1994) 1401–1405.

[19] S.P. Gurav, J.F.L. Goosen, F. VanKeulen, Bounded-but-unknown uncertainty optimization using design sensitivities and parallel computing: application to MEMS, Comput. Struct. 83 (2005) 1134–1149.

[20] C. Jiang, X. Han, G.R. Liu, Optimization of structures with uncertain constraints based on convex model and satisfaction degree of interval, Comput. Methods Appl. Mech. Engrg. 196 (2007) 4791–4800.

[21] X. Guo, W. Bai, W.S. Zhang, X.X. Gao, Confidence structural robust design and optimization under stiffness and load uncertainties, Comput. Methods Appl. Mech. Engrg. 198 (2009) 3378–3399.

[22] X. Guo, J.M. Du, X.X. Gao, Confidence structural robust optimization by nonlinear semidefinite programming-based single-level formulation, Internat. J. Numer. Methods Engrg. 86 (2011) 953–974.

[23] X. Guo, W. Bai, W.S. Zhang, Confidence extremal structural response analysis of truss structures under static load uncertainty via SDP relaxation, Comput. Struct. 87 (2009) 246–253.

[24] A. Takezawa, S. Nii, M. Kitamura, N. Kogiso, Topology optimization for worst load conditions based on the eigenvalue analysis of an aggregated linear system, Comput. Methods Appl. Mech. Engrg. 200 (2011) 2268–2281.

[25] B. Hassani, E. Hinton, A review of homogenization and topology optimization I—homogenization theory for media with periodic structure, Comput. Struct. 69 (1998) 707–717.

[26] S. Dempe, J. Dutta, Is bilevel programming a special case of a mathematical program with complementarity constraints?, Math. Program. A 131 (2012) 37–48.

[27] S. Boyd, L. Vandenberghe, Convex Optimization, Cambridge University Press, Cambridge, 2004.

[28] A. Shapiro, First and second order analysis of nonlinear semi-definite programs, Math. Program. 77 (1997) 301–320.

[29] O. Sigmund, On the design of compliant mechanisms using topology optimization, Mech. Struct. Mach. 25 (1997) 495–526.

[30] W.S. Zhang, W.L. Zhong, X. Guo, An explicit length scale control approach in SIMP-based topology optimization, Comput. Methods Appl. Mech. Engrg. 282 (2014) 71–86.

[31] K. Svanberg, The method of moving asymptotes—a new method for structural optimization, Internat. J. Numer. Methods Engrg. 24 (1987) 359–373.

[32] K. Fujisawa, M. Kojima, K. Nakata, M. Yamashita, SDPA User's Manual Version 6.0.

[33] O. Sigmund, Materials with prescribed constitutive parameters: an inverse homogenization problem, Int. J. Solids Struct. 31 (1994) 2313–2329.

[34] J. Aizenberg, J.C. Weaver, M.S. Thanawala, V.C. Sundar, D.E. Morse, P. Fratzal, Skeleton of euplectella sp. structural hierarchy from the nanoscale to the macroscale, Science 309 (2005) 275–277.